Strain induced anisotropies in silica polydimethylsiloxane composites

G. J. Schneider, and D. Göritz

Citation: The Journal of Chemical Physics **133**, 024903 (2010); doi: 10.1063/1.3447919
View online: https://doi.org/10.1063/1.3447919
View Table of Contents: http://aip.scitation.org/toc/jcp/133/2
Published by the American Institute of Physics

Strain induced anisotropies in silica polydimethylsiloxane composites

G. J. Schneider[1,a] and D. Göritz[2]
[1]*Institut für Festkörperforschung, Neutronenstreuung and Jülich Centre for Neutron Science, Forschungszentrum Jülich, 52425 Jülich, Germany*
[2]*Institut für Physik, Universität Regensburg, 93040 Regensburg, Germany*

(Received 31 August 2009; accepted 13 May 2010; published online 14 July 2010)

Structural changes of silica in polydimethylsiloxane rubber induced by external forces were studied by means of small-angle X-ray scattering experiments. The silica fraction varies from 9 up to 23 vol% and the elongation ratio from 1 to 3. Within the q-range of 0.02 $nm^{-1} < q < 1$ nm^{-1} the primary particles and the clusters which consist of these basic units could be resolved. The scattering diagrams of the samples without external deformation are radially symmetric and, in particular, the mass fractal dimension does not depend on the silica fraction. Due to the deformation the contours of the two-dimensional scattering diagrams become elliptic. A model independent analysis of the intensity as a function of the q-vector perpendicular and parallel to the deformation axis revealed that the microscopic cluster size is systematically increased by the macroscopic external deformation. In particular, the deformation ratio at the microscopic and the macroscopic length scale is very similar. The mass fractal dimension, as obtained by the slope of the scattering curve, increases significantly with growing deformation ratio, but is the same in vertical and horizontal directions. A simple relation derived for the crossover from self-similar to self-affine fractals can be used to relate the cluster sizes perpendicular and parallel to the deformation and the mass fractal dimension. By that means, it is demonstrated that the mean number of particles within each aggregate is constant, although the rubber was stretched up to a factor of 3. © *2010 American Institute of Physics*. [doi:10.1063/1.3447919]

I. INTRODUCTION

Polymer composites are indispensable for the daily life. One reason might be the outstanding variety of materials, which is achieved by a combination of soft polymer matrices and hard particles, to account for almost all sorts of applications. For example, the permeability and selectivity of polymer membranes can be changed using nanoparticles.[1–4] In the case of silica and carbon black composites a significantly higher modulus of the composite, a so-called reinforcement effect, is achieved.[5–10] In contrast, a decrease of the viscosity is found if very small particles are added.[11–13] However, even after several decades of intense scientific research a comprehensive knowledge of the correlation between the macroscopic properties, e.g., the viscosity of a mixture, and of the microscopic structure is still missing. In particular, in context with this question the change of the morphology at the microscopic length scale due to the application of external force fields is of interest.

Pure polymer melts have been exhaustively characterized, in particular, by small-angle neutron scattering experiments and connected to the theory of polymers.[14–19] By that means the microscopic deformation of the chains due to the deformation of the macroscopic sample was evidenced. As illustrated by the above examples, the mixtures of hard particles and soft matrices exhibit different properties if compared to the pure polymer. Therefore, if the microscopic structure shall be fully correlated with the macroscopic response, both the characterization of the polymer and the particle phase is necessary.

In the case of carbon black the reinforcement effect was first explained by the formation of a network of particles.[20,21] Therefore, the present work focuses on the important question how do external forces, mediated by a polydimethylsiloxane (PDMS) rubber matrix, change the silica morphology. If hard particles are mixed with a soft matrix, then one would probably expect that only the polymer chains can be deformed by the external force. However, as demonstrated, e.g., Ref. 22, silica consists of a hierarchical structure, i.e., the primary particles form clusters, which are the basic units for larger clusters. If an external force is applied to silica, then the clusters will be deformed, e.g., Refs. 23–25. In particular, it is found that due to the stretching of the polymer matrix, the structure of the clusters can be changed, e.g., Refs. 26–28.

Recently, an increase of the mass fractal dimension due to the external deformation was reported.[27,28] In contrast microscopic experiments reveal a decrease of the mass fractal dimension if one single cluster is deformed, e.g., Refs. 25 and 29. Studies on carbon black suggest that the filler fraction seems to influence the mass fractal dimension.[26] Therefore, the question arises whether cluster-cluster interactions can influence the mass fractal dimension systematically and thus explain the contradictions between the different experiments.

The present work studies the possible appearance of anisotropies in polymer silica composites using the small-

[a]Electronic mail: g.j.schneider@fz-juelich.de.

angle X-ray scattering (SAXS) technique and thus focusing on the hard particle phase. Such experiments are very well suited to obtain a precise knowledge on the morphology.[30] Due to the benefit of two-dimensional detectors a detailed study of the anisotropy is possible, and in this case a possible change of the morphology can be directly observed.[26,31] However, frequently one-dimensional cuts in the directions parallel and perpendicular to the deformation are very convenient. In particular, because if the cuts are plotted as a function of the momentum transfer in a double-logarithmic representation, the slope can be directly related to the mass fractal dimension[28,30,32] and therefore, to possible changes due to external forces.

The mechanical properties depend not only on the particles, rather than on the particle fraction.[5–10] Up to now a detailed study of the change of the morphology or on the structural changes due to external forces correlated with a systematic variation of the particle fraction is missing. Therefore, in order to contribute to a better knowledge of composite materials, the present paper focuses on the influence of the filler concentration on the microscopic structural changes induced by the external deformation. For this purpose external forces are applied on silica PDMS rubber composites and the structural changes are followed by means of SAXS experiments. Within the q-range of $0.02\ \mathrm{nm}^{-1} < q < 1\ \mathrm{nm}^{-1}$, the primary particles and the clusters which consist of these basic units could be resolved. As shown below, the silica-PDMS composite is most suitable for studying the open questions because without the application of external forces the scattering diagrams are radially symmetric, and, in particular, the mass fractal dimension does almost not depend on the silica fraction. Thus, the external deformation can be directly related to the scattering diagrams. Due to the variation of the silica fraction the contributions of cluster-cluster interactions to the mass fractal dimension can be studied.

II. EXPERIMENTAL SECTION

A. Samples

The PDMS $(SiO(CH_3)_2)_n$ rubber filled with precipitated silica VN3 was kindly provided by Lanxess (Leverkusen, Germany). Detailed descriptions of the precipitated silica and its synthesis are available in several reviews.[10,33,34] The volume fraction of the filler varies from 9 to 23 vol%. To cure the rubbers the manufacturer used 0.4 phr Varox 50 and heated the mixtures 10 min at 175 °C using a press. Then the samples were vulcanized 10 min at 170 °C and annealed 6 h at 200 °C.

B. SAXS experiments

The SAXS experiments were performed at the beamline BW4 of the DORIS III storage ring at the Hamburger Synchrotronstrahlungslabor (HASYLAB) at the Deutsches Elektronen-Synchrotron (DESY), Hamburg (Germany). The measurements using the standard transmission configuration[35,36] were carried out at a fixed energy of 8979 eV, corresponding to a wavelength $\lambda_{\text{X-ray}}=0.138$ nm. The scattered intensity was recorded by the two-dimensional Gabriel-type detector. The intensity I as function of q (or q_x and q_y) was obtained by radially averaging over a 20° wide segment of a circle. To enlarge the accessible range of momentum transfer q [$q=(4\pi/\lambda_{\text{X-ray}})\sin\theta$, where 2θ is the scattering angle] and thus the accessible length scale, different sample-detector distances (2 and 12 m) were combined. In order to achieve sufficient statistics and to avoid detector overflow, the scattering diagrams are accumulated 360 s (12 m) and 600 s (2 m).

The stretching experiments were performed using an apparatus provided by Heise *et al.* (Universität Ulm, Ulm, Germany). Each X-ray experiment starts using a virgin sample and without the application of external forces. Then the rubber was clamped in the stretching unit and measured again. Since there are no differences between the scattering diagrams of both measurements, this case is referred to as $\Lambda=1$. The elongation ratio Λ is defined by

$$\Lambda = \frac{l}{l_0}, \tag{1}$$

where l_0 is the initial length of the sample and l is the length of the deformed rubber. As suggested by supplementing experiments (not shown in this work), a relaxation of the silica structure, i.e., a change of the scattering diagram during the measurements, becomes important if the samples would be fully released, i.e., for example, if the surrounding rubber tears during the X-ray experiment. This agrees very well with results of transmission electron microscope (TEM) experiments.[23–25,29,37–40] In order to avoid such kind of relaxation phenomena, the elongation ratio is kept constant during the data acquisition.

III. THEORY

The silica studied by the present work consists of primary particles which form aggregates due to the high volume concentrations of the samples involved. The aggregates are the basic units for larger clusters. By that means a hierarchical structure, consisting of several characteristic length scales, is generated. Such an object can be reasonably well described by the concept of fractals. Therefore, most conveniently the scattering diagrams of silica can be analyzed. The measured intensity I can be decomposed in the particle factor P, i.e., scattering of the primary particles and the structure factor S that describes the arrangement of the particles within the aggregates by $I \propto SP$.[30,41]

If the growth process of the clusters is isotropic, a self-similar object is obtained for which the simple scaling relation,

$$N = a\left(\frac{\xi}{r}\right)^{d_m}, \tag{2}$$

is applicable.[42] N is the number of primary particles with radius r within the aggregate of radius ξ. The prefactor a is denoted as lacunarity and it has been shown that $a \approx 1$.[43] Therefore, for convenience it is assumed that $a=1$ hereafter. The mass fractal dimension d_m represents the cluster branching. For example, if the object is linear then $d_m=1$. When a

homogeneous sphere is considered then $d_m=3$. Using Eq. (2) the scattered intensity I,

$$I \propto q^{-d_m}, \tag{3}$$

can be calculated.[30] If the cluster, initially fully isotropic, i.e., spherically symmetric, is deformed, the situation changes. The modeling of the cluster by a simple self-similar fractal is no longer feasible, rather than the theory of self-affine fractals has to be applied.[42] As reported recently by Roldughin,[44] then the simple scaling relation, Eq. (2), has to be replaced by

$$N = \left(\frac{\xi_a}{r}\right)^{d_a} = \left(\frac{\xi_b}{r}\right)^{d_b} = \left(\frac{\xi_c}{r}\right)^{d_c}, \tag{4}$$

with ξ_a, ξ_b, and ξ_c representing the half length of the minor and semiaxis of an elliptically shaped cluster, and d_a, d_b, and d_c are three individual fractal dimensions. It is worth to mention that the self-affine scaling includes the case that the primary particles are not spherically symmetric. However, the forces applied below to deform the clusters are very weak in comparison to those related to the chemically bonded SiO_2-molecules which form the silica primary particles. Therefore, it is assumed that the primary particles are initially fully spherically symmetric and do not change their shape due to the external forces, which is implicitly assumed in Eqs. (4).[28,32] As will be shown below, this assumption is confirmed by the experimental results.

In the case of $a=1$ it is possible to rewrite Eqs. (4) by[44]

$$N = \left(\frac{(\xi_a \xi_b \xi_c)^{(1/3)}}{r}\right)^d \tag{5}$$

and thus characterizing the self-affine fractal by one fractal dimension, defined by Eq. (5), only. If it is assumed that the number of particles within the cluster is constant during the deformation, then the right hand sides of Eqs. (2) and (5) are identical, and thus[28]

$$d = d_m \frac{1}{(1 + 1/3(\log(\lambda_b^2 \lambda_c)/\log(\xi/r))}. \tag{6}$$

Without restricting the generality, it is assumed that the deformation is symmetric and hence $\lambda_a=\lambda_b$, where $\lambda_a=\xi_a/r$ and $\lambda_b=\xi_b/r$ are the microscopic deformation ratios, which are not necessarily connected to the macroscopic elongation ratio.[28] Therefore, if the cluster is deformed without breaking or without loosing particles, the fractal dimension of the self-affine object is directly related to the known mass fractal dimension of the corresponding self-similar object. Furthermore, as a consequence of Eq. (5) the scattered intensity is given by[32]

$$S(\tilde{q},\xi,r_0,d) = 1 + (\lambda_b^2 \lambda_c)^{d/3} \cdot \frac{\Gamma(d+1)}{(\tilde{q} r_0)^d} \cdot \left(1 + \frac{1}{(\tilde{q}\xi)^2}\right)^{(1-d)/2} \cdot \frac{\sin[(d-1)\arctan(\tilde{q}\xi)]}{(d-1)}, \tag{7}$$

with the gamma function Γ and the abbreviation

$$\tilde{q} = q\sqrt{\lambda_b^2 \sin^2 \alpha + \lambda_c^2 \cos^2 \alpha}. \tag{8}$$

Oh and Sorensen[45] derived a simple relation between the radius of gyration of the cluster with an arbitrary mass fractal dimension and its perimeter radius R,

$$\xi^2 = 2d_m(d_m+1)/((d_m+2)(d_m+5))R^2. \tag{9}$$

In the simple case of a homogeneous spheres with $d_m=3$, the relation $R^2=5/3R_{g^2}$ is obtained.

Neglecting the physical size limits, the intensity is given by

$$I \propto \tilde{q}^{-d}. \tag{10}$$

Therefore, in the ideal case of the deformation of a fractal, i.e., neglecting breaking and rupturing effects, the slope of the intensity as a function of the q-values is given by the fractal dimension within a log-log plot. However, it is very important to mention that Eq. (7) is valid even if breaking and rupturing of the clusters occur. Under these circumstances only the simple relation to the undeformed fractal, via the number of particles in the cluster, is violated. However, and this is most remarkably, the slope does not depend on the direction of the cut. In the simple case, the slope can be calculated by Eq. (6), and thus, e.g., predicting the increase of the slope due the deformation of the cluster.[28]

Similar to the modeling of the clusters by mass fractals, the surface of the primary particles can be represented by the so-called surface fractal dimension d_s.[46] For example, if the surface is smooth $d_s=2.0$ and if $d_s=3.0$ the surface is infinitely rough.[30] The scattered intensity of a fractal surface is simply[30]

$$I \propto q^{-(6-d_s)}. \tag{11}$$

Therefore, both the mass and the surface fractal dimension can be obtained by a simple log-log plot of the intensity as a function of the q-value. Fortunately the slopes usually observed are different and therefore, the mass and surface fractal ranges can be distinguished very easily.

Frequently the particles involved are polydisperse. Therefore, characteristic oscillations, representing the diameter, which would be observed in the scattering diagrams in the case of monodisperse particles, are smeared out. However, then the positions of the crossovers q_c between the fractal ranges provide an approximative value for the radius r by $r=\pi/q_c$.[47] One convenient way to determine r is to fit the intensity with the particle factor of Rayleigh or its approximations, e.g., the approach of Beaucage.[46] However, as will be evident below, in the particular case shown, it is difficult to determine the cluster size from such a fit because the related q_c is very close to the edge of the experimentally resolvable q-window. Therefore, a different technique is used instead.

IV. RESULTS AND DISCUSSION

Figure 1 shows the two-dimensional scattering diagrams, i.e., the contour plots of the scattered intensity as a function of the q_x- and q_y-axes. The silica fraction varies from 9 to 23 vol%. To prevent the detector from the intense undiffracted synchrotron radiation, a beam stop is placed in the middle

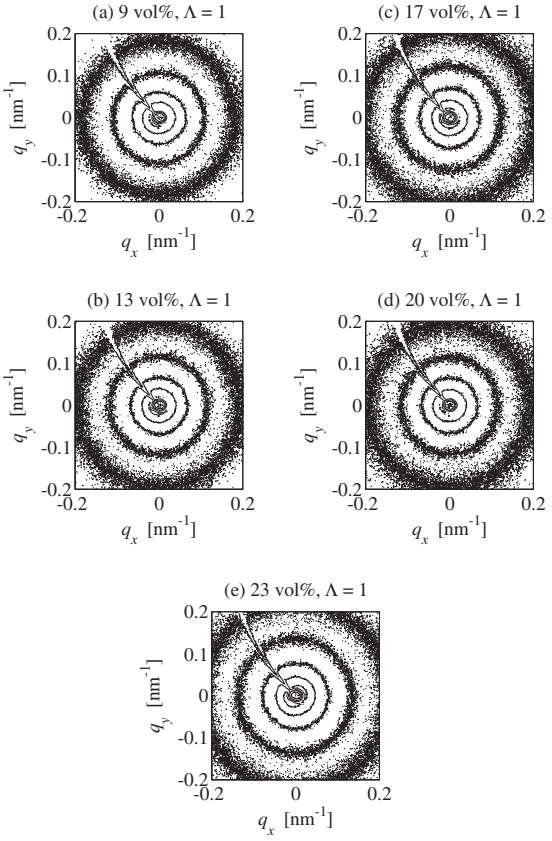

FIG. 1. Two-dimensional scattering diagrams of silica (9–23 vol%) in PDMS.

position. Its holder is visible at the upper left side of each diagram. As will be revealed below possible asymmetries can be observed at small q-values only. Therefore, only the range $|q| \leq 0.2$ nm^{-1} is depicted. Each of the scattering diagrams shown in Fig. 1 is radially symmetric. Slight distortions appear only at the very low q-values and are neglected hereafter because they might be due to the proximity to the beam stop or its holder.

The one-dimensional cuts, i.e., the intensity $I(q_x,0)$ and $I(0,q_y)$ referred to as horizontal and vertical cuts, respectively, are depicted in Fig. 2. Here and later only those intensity values are plotted and used for the analysis, which are not influenced by the beam stop. In order to analyze the primary particles as well as the clusters, a larger q-range, in comparison to the two-dimensional plots, is depicted. The

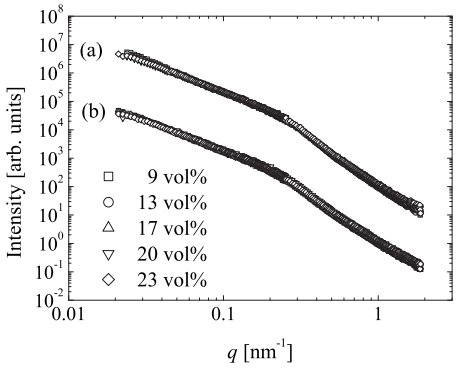

FIG. 2. Comparison of (a) horizontal and (b) vertical cuts.

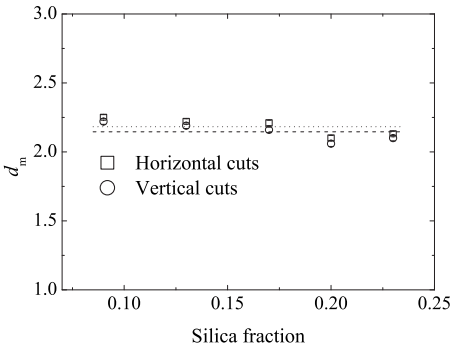

FIG. 3. Mass fractal dimension d_m as a function of the silica fraction obtained analyzing the horizontal and vertical cuts. The dotted and the dashed lines represent the average values for the horizontal and vertical cuts, respectively.

cuts demonstrate that the intensity decays with increasing q-values, but they do almost not depend on the silica fraction. In particular, the slopes are only very slightly influenced.

As explained above, because of its physical origin, the diagrams can be divided into two q-ranges: the surface fractal range at large and the mass-fractal regime at small q-values. The crossover q_c reflects the size of the primary particles. From the range $0.4\ \text{nm}^{-1} < q < 1\ \text{nm}^{-1}$ a constant surface fractal dimension $d_s = 2.0 \pm 0.01$ is revealed. The position of q_c does not depend on the filler fraction nor on the direction of the cut. Fitting the intensity as described in Sec. III a radius of gyration $R_g = 8.7 \pm 0.1$ nm and hence a perimeter radius $r = 11.2 \pm 0.1$ nm is obtained.

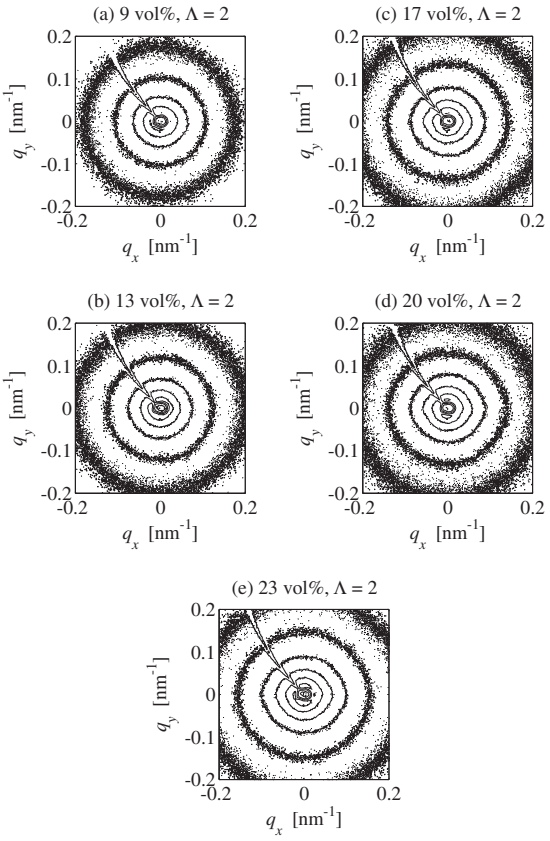

FIG. 4. Two-dimensional scattering diagrams of silica (9–23 vol%) in PDMS. The polymer matrix is stretched by a factor $\Lambda = 2$.

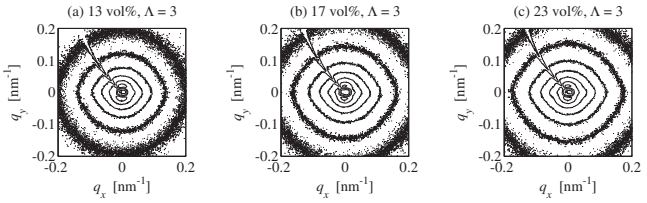

FIG. 5. Two-dimensional scattering diagrams of silica (9–23 vol%) in PDMS. The polymer matrix is stretched by a factor $\Lambda=3$.

There is a slight dependency on the silica fraction of the slope within $0.02\ \text{nm}^{-1} < q < 0.2\ \text{nm}^{-1}$. This is illustrated by Fig. 3, which shows the mass fractal dimension d_m as a function of the silica fraction and of the two different directions of the cuts. The slope was determined by using Eq. (3). The fitting error is 0.01 or below, and therefore, the error bars are very small and within the symbol size and almost not visible. This again demonstrates that the mass fractal dimension does almost not depend on the silica fraction but, in particular, no systematic dependency is visible.

Actually, the chosen fitting intervals are a compromise between the largest possible range and the perturbations due to the influence of the crossovers. Furthermore, scattering diagrams of fractals usually show deviations from the simple exponential decay or the linear decay in the log-log representation.[48] Therefore, if the q-range is varied, the results obtained by the local fit are changed, with differences greater than the fitting error given in the figure, which will become obvious below. However, if the fitting range remains constant for all of the fits, only the absolute values are affected, but not the conclusions drawn out of the relative values.

The average values obtained for the horizontal cuts $d_m=2.18$ and the vertical cuts $d_m=2.15$ agree very well. The difference is very weak, and therefore, no attempt is made to relate it to anisotropies in the sample or to other sources, e.g., to detector sensitivity.

In Fig. 2 a crossover to a Guinier range or to larger clusters is not visible at the small q-values, and therefore, even by using Eq. (7), the cluster radius cannot be determined. However, a first order estimation of a minimum size of $\xi=28$ nm is possible, by applying Eq. (7) and using $\lambda_b=\lambda_c=1$. By Eq. (9) and the mean value of $d_m=2.17$, a minimum perimeter radius $R=41$ nm is obtained. Thus the scaling relation, Eq. (2) ($a=1$), gives a minimum number of primary particles within the aggregates of $N=13-17$. This is in the range of 10–100, which seem to be the typical number of particles in aggregates.[49] It is worth to mention that there are several procedures to obtain the aggregation number N, even there are several possibilities for calculating it from the scaling relation.[30,50,51] However, the following discussion does not rely on differences in the absolute value due to the different ways and therefore, possible consequences are not considered further. Together with the radially symmetric scattering diagrams shown in Fig. 1, within the experimental error and the accuracy of the analysis, the samples can be referred to as isotropic. However, below it will be demonstrated that even these samples are slightly anisotropic, but this effect is very weak in comparison to the stretched samples.

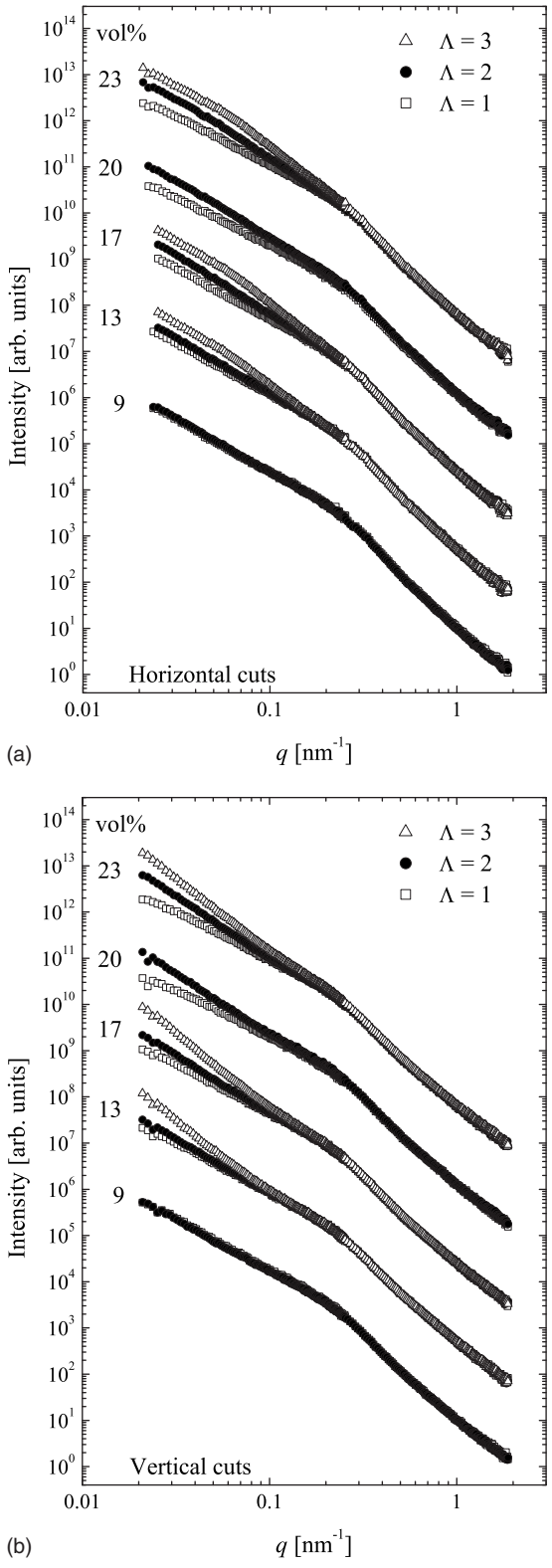

FIG. 6. The scattered intensity (a) $I(q_x,0)$ and (b) $I(0,q_y)$ of the silica (9–23 vol%) in PDMS for different elongation ratios.

Figure 4 shows the influence of the deformation of the rubber matrix by a factor of 2 on the silica in PDMS for the different filler fractions. The direction of deformation is always parallel to the q_y-axis, i.e., to the vertical direction. The

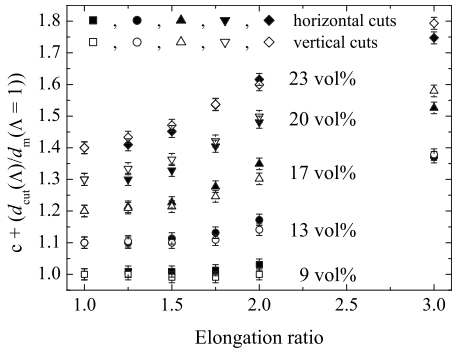

FIG. 7. Mass fractal dimension $d_m(\Lambda)$ of the horizontal and the vertical cuts as a function of the elongation ratio divided by $d_m(\Lambda=1)$ of the unstretched sample. For clarity a constant c is added. ($c=0$, 0.1, 0.2, 0.3, and 0.4 for 9,13,17, 20, and 23, respectively.)

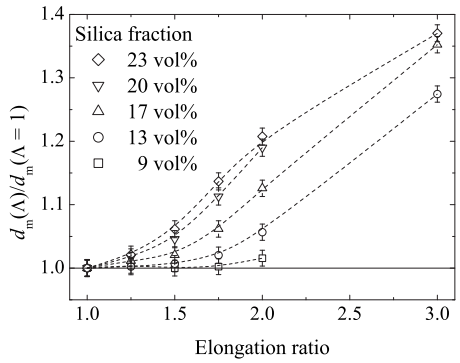

FIG. 8. Mass fractal dimension $d_m(\Lambda)$ as a function of the elongation ratio Λ divided by $d_m(\Lambda=1)$ of the unstretched sample. The dotted lines serve as guides for the eyes.

contours at small $|q|$-values exhibit weak asymmetries. Very slightly the deviations from the radially symmetric patterns become stronger with larger silica fractions. Furthermore, very close to the beam stop two "banana-like" shapes are visible in Fig. 4(e). It seems that this pattern disappears with decreasing silica fraction. At large $|q|$-values for all of the samples radially symmetric patterns are observed.

Figure 5 shows the influence of stretching the samples by a factor of 3. The 9 and the 20 vol% samples teared during deforming from $\Lambda=2$ to 3, and therefore, there are no scattering diagrams. Each of the diagrams exhibits pronounced asymmetries. At this elongation ratio the banana-like shapes appear even at 13 and 17 vol%. However, a systematic dependency on the silica fraction is not visible. At largest $|q|$-values the patterns are still radially symmetric.

The two-dimensional scattering diagrams reveal that the clusters are aligned due to the external force. Furthermore, the patterns demonstrate that the clusters become larger in the direction of the external force and smaller in the perpendicular direction if compared to the radially symmetric contours of the sample without external deformation. However, there is no remarkable effect on the elliptic contours due to the silica fraction.

Figure 6 depicts the influence of the external deformation by means of (a) the horizontal and (b) the vertical cuts. Due to the external force the intensity at $q<q_c$ is changed but not at the large q-values. In particular, the range $0.2\ \text{nm}^{-1}<q<0.3\ \text{nm}^{-1}$ which represents the size of the primary particles is not affected. Therefore, without assuming a particular model function it can be safely concluded that the radius of primary particles is not changed due to the deformation.

The cuts connected to the deformation ratio $\Lambda=2$ demonstrate that the change of the mass fractal dimension is correlated with the silica fraction. The main effect is the change of the slope of the intensity, but additionally a change of the curvature is visible. Remarkably the curvature of the intensity is opposite if the vertical and the horizontal cuts are compared. From this result it is evident that the simple assumption of a linear decay in the double-logarithmic representation suggested by Eq. (3) cannot account for the experimental data fully. However, the scattering diagrams of hierarchical structures are not very well understood. Therefore, first, a simple analysis by fitting Eq. (3) is attempted as it is common in the literature, e.g., the textbook of Bunde and Havlin,[30] but afterwards the cuts are analyzed more in detail, to reveal the different features involved step by step.

Figure 7 depicts the changes in the mass fractal dimension as a function of the macroscopic elongation ration Λ. For the sake of clarity the individual values are shifted by a constant value on the d_m-axis. Clearly, the mass fractal dimension increases systematically with increasing Λ. However, the slope of the horizontal and the vertical cuts is almost the same, as expected by relation (7). In order to better visualize the dependency of the mass fractal dimension on the silica fraction and the elongation ratio, Fig. 8 depicts the mean value of the mass fractal dimension of the horizontal and the vertical cuts as a function of Λ. The dotted lines serve as a guide for the eye and demonstrate that there is a pronounced dependency on the silica fraction. Remarkably, d_m of the sample with a silica fraction of 9 vol% does almost not depend on the elongation ratio, as illustrated by the constant line, which represents the mean value of the unstretched sample.

In order to reveal further details, Fig. 9 depicts the horizontal cuts of the sample with 23 vol% silica in a Kratky-like representation, i.e., Iq^d as a function of q. Here and below d is the individual value for each scattering diagram. Of

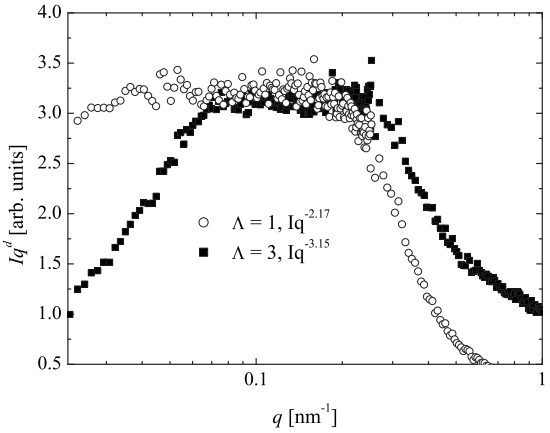

FIG. 9. Kratky-like representation of the horizontal cuts of the sample with 23 vol% silica.

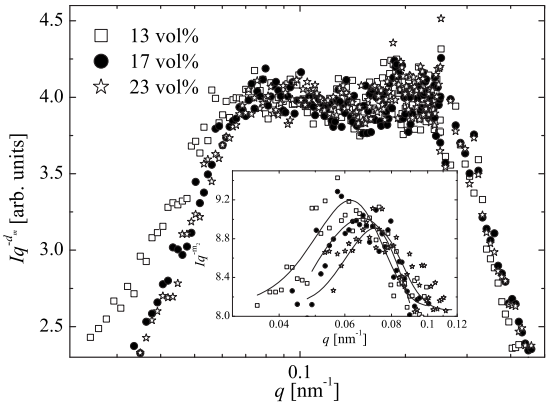

FIG. 10. Comparison of the Kratky-like representations of the horizontal cuts of samples with different silica fractions at $\Lambda=1$. The inset shows the same data in the representation Iq^{m2} as a function of q. m_2 represents the mean value of the slopes at $q<q_c$ and $q>q_c$ and by that means allowing a fit by a Gaussian distribution visualized by the lines. In the inset the intensities are slightly shifted arbitrarily for the sake of clarity.

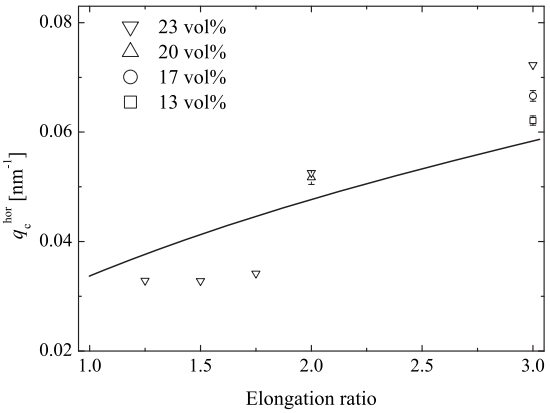

FIG. 11. The crossover at small q's vs the elongation ratio. The line depicts the estimation of q_c^{hor} by the macroscopic elongation ratio.

course, this illustration results in differences at the high-q side which therefore, not to be considered further. The Kratky-like representation evidences that at the small q-values there is a slope which is different from that in the middle range. Therefore, a crossover q_c^{hor} is generated which does not exist at $\Lambda_c=1$. If one assumes that the size of the cluster is outside the q-window initially, then due to the deformation of the surrounding polymer, obviously the cluster is compressed. Most remarkably, this crossover is almost invisible in the log-log representation of the intensity as a function of the q-value depicted in Fig. 6(a), but clearly present as revealed by the Kratky-like plot.

Figure 10 shows a comparison of the Kratky-like representations of the samples with different silica fractions. The differences are very small. In order to resolve them, the inset shows a Kratky-like representation with Iq^{m_2}, where m_2 is the mean value of the dimension obtained on the right and left hand sides of the crossover. As suggested by Ref. 26 by using simply a Gaussian interpolation function, then an accurate determination of q_c is possible, without relying on a particular model function. This is shown in the inset, where the curves are arbitrarily shifted a little bit in the vertical direction for the sake of clarity. It shows that there is a very slight dependency, which is depicted in Fig. 11 for all of the vertical cuts where a crossover can be clearly resolved. The line shows the prediction for the sample dimension of the polymer, just by assuming $\Lambda_b^2\Lambda_c=1$ and assuming $q_c(\Lambda=1)=0.033$ nm^{-1}, which is the mean value of the three q_c values of the 23 vol% sample at the lowest elongation ratios. However, since the q_c for $\Lambda=1$ is not visible, this is an first order approximation, which is only confirmed later. Although there are pronounced differences between the prediction and the experimental data points, the overall increase of q_c with the sample deformation is sustained. Therefore, the crossover is clearly related to the cluster size perpendicular to the deformation, and the above observation of a decreasing cluster size in the perpendicular direction with increasing deformation ratio is confirmed. It is worth to note that the difference of the experimental q_c and the calculated line is larger if the silica fraction is higher. Unfortunately, the q_c's of the samples with lower silica fraction become visible only at larger elongation. Therefore, it is not possible to quantify this effect further. Hence it is not possible to decide whether the different q_c's at $\Lambda=3$ are generated due to the filler fraction, i.e., by the distance between the objects, or by the clusters themselves, likely to be larger at the smaller silica concentrations.

The Kratky-like plots of the vertical cuts is depicted in Fig. 12. Clearly, at some elongation ratios two different features, which can be referred to as two different crossovers,

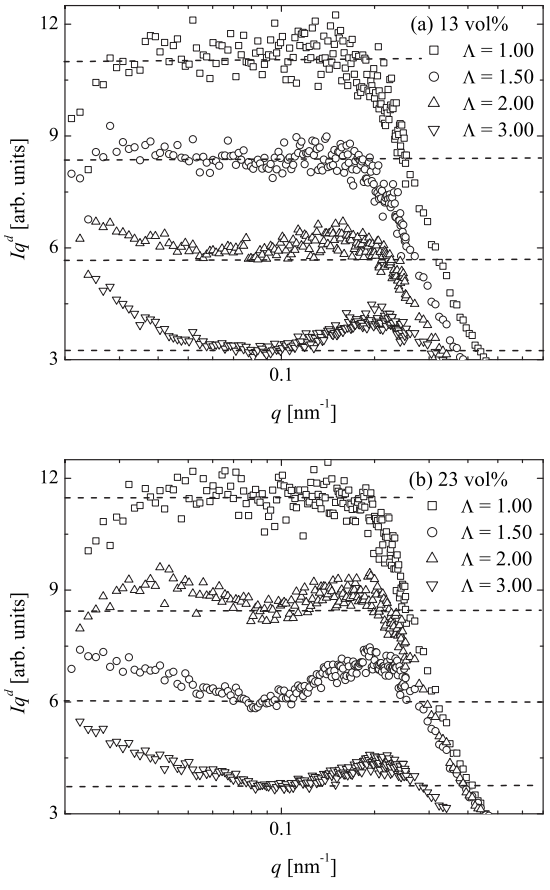

FIG. 12. Kratky-like representation of the vertical cuts (a) 13 vol% and (b) 23 vol%.

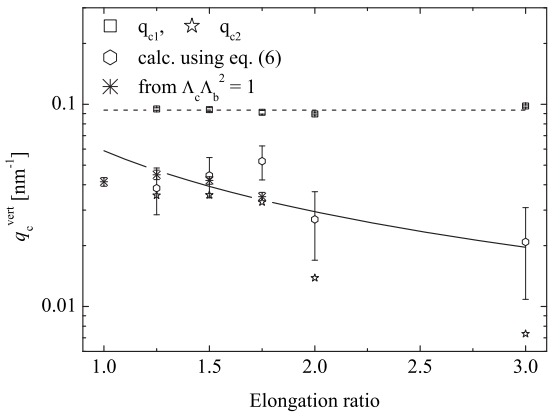

FIG. 13. Crossover q_c^{vert} as obtained by fitting a Gaussian function to the local minima and maxima visible in Fig. 12. Only those values are included where the crossover can be clearly identified. The line represents the expectation if the cluster size changes with the macroscopic elongation ratio. The dotted line stands for the mean value of the q_c^{vert}.

are visible. Due to the deformation, obviously a crossover at about 0.09 nm^{-1} is generated. Its strength depends on the deformation ratio as well as on the silica fraction, but obviously its position remains constant. Furthermore, at the low elongation ratios a second crossover is visible. In the case of the unstrained sample the Kratky-like representation in perpendicular direction does not display such a crossover. Therefore, this is an indication of a small anisotropy. Since this isn't visible in the two dimensional scattering diagrams it is neglected hereafter. In order to quantify the crossovers, q_c^{vert} is obtained by fitting a Gaussian function as described before and is depicted in Fig. 13. For the sake of clarity, and since there is no new information, only the 23 vol% sample is displayed, whereas the others are intentionally left out. The line depicts the macroscopic deformation in the reciprocal space, i.e., $q_c(\Lambda=1)/q_c^{vert}(\Lambda)=c(\Lambda)/c(\Lambda=1)=\Lambda_c$. Since the unstretched sample is anisotropic, $q_c^{vert}(\Lambda=1)=0.059\pm0.004$ nm^{-1} was determined by fitting the data. This value is very close to the experimental value of $q_c^{vert}(\Lambda=1)=0.041\pm0.002$ nm^{-1} from the vertical cuts. In particular, it describes the dependency of q_c^{vert} on Λ sufficiently well. Therefore, this is a first indication that this crossover is correlated with the cluster deformation.

Above, q_c^{hor} was clearly related to the external deformation. By means of the simple relation $\Lambda_c\Lambda_b^2=1$, the expectation for the cluster size in vertical direction can be estimated from the crossovers in the horizontal plots. However, as can be seen in Fig. 13, whereas the prediction works very well at the small elongation ratios at the higher amplitudes, the prediction completely fails. In particular, the estimation of the microscopic deformation ratio by the ratio of the q's at $\Lambda=3$ and $\Lambda=1$ is about 8, which is very unlikely. Already, if Fig. 11 is considered, then at the highest elongation ratio a pronounced difference will be visible. Therefore, the question arises, whether the macroscopic relation $\Lambda_b^2\Lambda_c=1$ is unable to predict the microscopic structural changes due to macroscopic deformation of the surrounding rubber or both crossovers are not related to each other. Hence, the discussion has to address the microscopic situation more in detail. This can be achieved exploiting Eq. (6), which relates the microscopic elongation ratios of the cluster, i.e., $\lambda_c=f(\lambda)/\lambda_b^2$. Obviously $f(\lambda)=10^{3(d(\lambda=1)/d(\lambda)-1)\log(R/r_0)}$ is a correction term resulting from the strict mathematical treatment, i.e., the crossover from self-similar to self-affine fractals. This relation can be used to calculate q_c^{vert} from q_c^{hor}. The result is shown in Fig. 13. The error bars are a result of the inaccuracy in the determination of the $q_c^{hor}(\Lambda=1)$. However, the result is very close to the line representing the macroscopic deformation. In particular, it is demonstrated that the cluster is deformed up to a factor of about 3 at the microscopic length scale which agrees very well with the macroscopic ratio. Furthermore, the simple relation predicts the validity of the macroscopic relation $\Lambda_c\Lambda_b^2=1$ in the particular case of a low filler fraction and low deformation ratio because then the mass fractal dimension is very close to the value of the unstretched sample. In the present case, even 9 vol% is low enough, because there, the mass fractal dimension does almost not depend on the particle fraction. Furthermore, it demonstrates that the clusters are compressed stronger if the silica concentration is higher, in comparison to the changes expected for the deformation of a pure rubber. In particular, the connection of the crossovers at the very low q-values of the vertical and horizontal cuts is therefore, evidenced. It is by far not self-evident that Eq. (6) is valid because it is achieved by assuming that the number of particles, at least the mean number of particles, within the cluster remains constant. However, in the particular case shown above this is obviously the case. Friedlander deformed pure nanoparticles and observed exactly the same behavior.[29] Of course, if the elongation ratios are large enough the cluster break and by that mean the (average) number of particles in the clusters decrease.

Finally, the second crossover, which, however, is only visible in the Kratky-like plots of the vertical cuts, has to be addressed. Usually, if such a crossover is visible a corresponding length scale is determined, e.g., Ref. 49. On the other hand, in the case of isotropic samples, other authors relate the curvature to the underlying fractal nature.[48] Figure 13 demonstrates that the corresponding q_c is not related to the deformation because its position is more or less constant, at least there is no systematic dependency on the filler fraction.

Figure 12 demonstrates that fitting the intensity $I(q<0.2$ nm$^{-1})$ by a straight line is possibly not sufficient. At least two different slopes can be identified. Figure 14 displays the two slopes obtained by linear fits of the scattering diagrams of the 23 vol% sample displayed in Fig. 6(b). The two ranges are approximately $q<0.1$ nm^{-1} and 0.1 nm$^{-1}<q<0.2$ 0.1 nm^{-1}. They are compared to the slope obtained by fitting the intensity in the whole range, i.e. $I(q<0.2$ nm$^{-1})$. There are differences, however, a common increase with growing deformation ratio is observed. Finally, a mass fractal dimension $d_{m2}\approx3.2$ is obtained. Clearly, this contradicts the assumption of the scattering of mass fractal objects. Already these two arguments contradict the assumption of an additional crossover related to a structural feature. Furthermore, if the scattering diagrams in Figs. 2 and 6 at the high q-values are considered, then there a similar curvature visible at around 0.3–0.5 nm^{-1}. In that case it is simply due

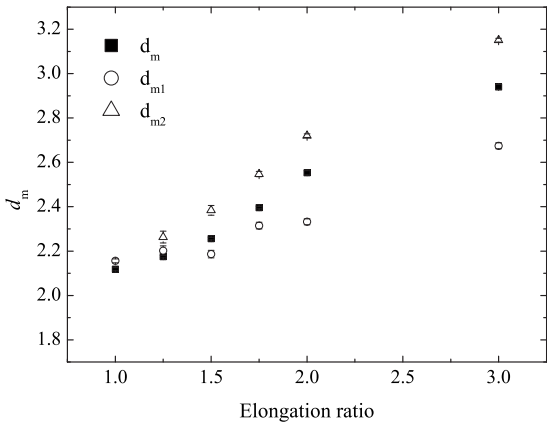

FIG. 14. The different mass fractal dimensions as a function of the elongation ratio resulting from the three different q-ranges: full range, d_m, i.e., from the minimum q visible to approximately 0.2 nm^{-1}, d_{m1} from the range on the right hand side of the minimum up to approximately 0.2 nm^{-1}, and d_{m2} from the range on the left hand side of the minimum.

to the smearing out of the oscillations due to polydispersity. This demonstrates that not only the fractal behavior rather than the polydispersity of the sample can result in such a curvature. Therefore, it is finally concluded that this crossover is not related to a separate structural feature. This, however, shows the importance of achieving very low q-values to understand hierarchical structures and, in particular, to decide whether it is a true crossover or simply a curvature.

V. CONCLUSION

It was demonstrated that the structure of the silica clusters can be changed by the external deformation of the rubbery matrix. The microscopic deformation ratios are related to the macroscopic elongation ratio. As described above the radius of the silica cluster was roughly 41 nm. Due to the stretching the cluster finally has sizes of about $c \approx 120$ nm parallel and $b \approx 20$ nm perpendicular to the direction of the deformation. Such deformation was similarly obtained using the TEM.[23–25,29,37–40] However, it was reported that the mass fractal dimension decreases due to the deformation, whereas above an increase was reported. The differences of the scattering and the TEM experiments are on the one hand the number of clusters involved and on the other hand the environment of the particles: the scattering experiments consider a very large number of objects, and of course their interactions, the cited microscopic experiments studied exactly one cluster. Furthermore, whereas the present work investigated silica in PDMS, the microscopic experiments have been performed on the pure silica. The above experiments demonstrated that the change of the mass fractal dimension is related to the filler fraction. Thus, it is likely that this would explain the differences. However, it is very difficult, if possible, to perform scattering experiments on one single cluster as well as to perform a rubber deformation experiment in the TEM. Studying low silica fractions in rubber by means of SAXS experiments could probably contribute to further solve this question.

The two-dimensional scattering diagrams at the elongation ratio of $\Lambda = 3$ (Fig. 5) show the onset of a so-called lozenge pattern. The deviations from the elliptical pattern are very small, and thus this does not affect or change the above analysis. However, it is an indication for a "polydispersity" of clusters.[32] Such an effect can be generated by a size distribution of the initial clusters, a size distribution of the primary particles, or/and a number distribution of the number of particles in clusters.[32] Furthermore, it could be the result of a nonaffine deformation of the polymer itself.[16,18] Moreover, due to the finite measurement time, it is possible that the polymer matrix relaxes and therefore, the average scattering pattern represents the average over different ratios. All of these effects, independently of each other, are able to create the deviations from the perfect elliptical shape, but it is very likely that all of them contribute to it. Therefore, it is very astonishing that only such weak deviations are visible.

Finally, the weak banana–like shaped patterns observed at very low q-values should be addressed. Although this shape seems to be due to the proximity to the beam stop, and therefore, artificial, it is predicted by simulations:[52] If the stretching ratio becomes higher, then the deformation is no longer affine, in particular, due to strain induced filler-filler interactions. Indeed this phenomenon would depend on the filler fraction and reflects the observation. Since the banana-like shapes appear only at the edge of the experimental window, no further discussion is attempted. However, it should be mentioned that the low q-values, at which the banana-like shapes are visible are not used for the above analysis because a decision between an artifact due to the proximity to the beam stop or a real effect could not be made.

ACKNOWLEDGMENTS

We gratefully acknowledge the help of Dr. Heise, Universität Ulm, Ulm, Germany, for supplying the tensile unit and supporting the experiments. We thank Sabine Cunis for the technical support of the SAXS experiments. Providing beam time and financial support of the experiments by the HASYLAB/DESY is gratefully acknowledged. We kindly thank, Leverkusen, Germany, for supplying the samples.

[1] T. C. Merkel, B. D. Freeman, R. J. Spontak, Z. He, L. Pinnau, P. Meakin, and A. J. Hill, Science **296**, 519 (2002).
[2] D. Gomes, S. Nunes, and K.-V. Peinemann, J. Membr. Sci. **246**, 13 (2005).
[3] R. Hill, Phys. Rev. Lett. **96**, 216001 (2006).
[4] J. Kruse, K. Rätzke, F. Faupel, D. M. Sterescu, D. F. Stamatialis, and M. Wessling, J. Phys. Chem. B **111**, 13914 (2007).
[5] G. Kraus, *Reinforcement of Elastomers* (Wiley, New York, 1965).
[6] J.-B. Donnet and A. Voet, *Carbon Black: Physics, Chemistry and Elastomer Reinforcement* (Dekker, New York, 1976).
[7] A. I. Medalia, Rubber Chem. Technol. **51**, 437 (1978).
[8] S. Wolff and M. J. Wang, *Carbon Black: Science and Technology*, 2nd ed. (Dekker, New York, 1993).
[9] M.-J. Wang, Rubber Chem. Technol. **71**, 520 (1998).
[10] H. D. Luginsland, *A Review on the Chemistry and the Reinforcement of the Silica-Silane Filler System for Rubber Applications* (Shaker, Aachen, 2002).
[11] M. E. Mackay, A. Tuteja, P. M. Duxbury, C. J. Hawker, B. Van Horn, Z. Guan, G. Chen, and R. S. Krishnan, Science **311**, 1740 (2006).
[12] A. Tuteja, M. E. Mackay, C. J. Hawker, and B. van Horn, Macromolecules **38**, 8000 (2005).
[13] N. Hao, H. Böhning, H. Goering, and A. Schönhals, Macromolecules **40**, 2955 (2007).
[14] J. Bastide, L. Leibler, and J. Prost, Macromolecules **23**, 1821 (1990).
[15] J. Bastide, F. Boué, E. Mendes, F. Zielinski, M. Buzier, G. Beinert, R.

Oeser, and C. Lartigue, in *Polymer Networks '91: Proceedings of the International Conference*, Moskau (UdSSR), edited by K. Dušek and S. I. Kuchanov (VSP, Utrecht, 1992), p. 119.
[16] D. J. Read and T. C. B. McLeish, Phys. Rev. Lett. **79**, 87 (1997).
[17] D. J. Read and T. C. B. McLeish, Phys. Rev. Lett. **80**, 5450 (1998).
[18] E. Straube, V. Urban, W. Pyckhout-Hintzen, and D. Richter, Macromolecules **27**, 7681 (1994).
[19] E. Straube, V. Urban, W. Pyckhout-Hintzen, D. Richter, and C. J. Glinka, Phys. Rev. Lett. **74**, 4464 (1995).
[20] A. R. Payne, J. Appl. Polym. Sci. **6**, 57 (1962).
[21] A. R. Payne, J. Appl. Polym. Sci. **7**, 873 (1963).
[22] D. W. Schaefer, T. Rieker, M. Agamalian, J. S. Lin, D. Fischer, S. Sukumaran, C. Chen, G. Beaucage, C. Herd, and J. Ivie, J. Appl. Crystallogr. **33**, 587 (2000).
[23] S. K. Friedlander, J. Nanopart. Res. **1**, 9 (1999).
[24] K. Ogawa, T. Vogt, M. Ullmann, S. Johnson, and S. K. Friedlander, J. Chem. Phys. **87**, 63 (2000).
[25] W. Rong, W. Ding, L. Mädler, R. S. Ruoff, and S. K. Friedlander, Nano Lett. **6**, 2646 (2006).
[26] F. Ehrburger-Dolle, M. Hindermann-Bischoff, F. Livet, F. Bley, C. Rochas, and E. Geissler, Langmuir **17**, 329 (2001).
[27] A. Botti, W. Pyckhout-Hintzen, V. Urban, J. Kohlbrecher, D. Richter, and E. Straube, Appl. Phys. A: Mater. Sci. Process. **74**, 513 (2002).
[28] G. J. Schneider, J. Chem. Phys. **130**, 234912 (2009).
[29] S. K. Friedlander, H. D. Jang, and K. H. Ryu, Appl. Phys. Lett. **72**, 173 (1998).
[30] A. Bunde and S. Havlin, *Fractals and Disordered Systems* (Springer-Verlag, Berlin, 1995), Vol. 2.
[31] F. Ehrburger-Dolle, F. Bley, E. Geissler, F. Livet, I. Morfin, and C. Rochas, Macromol. Symp. **200**, 157 (2003).
[32] G. J. Schneider and D. Göritz, J. Appl. Crystallogr. **43**, 12 (2010).
[33] B. B. Boonstra, H. Cochrane, and E. M. Dannenberg, Rubber Chem. Technol. **48**, 558 (1975).
[34] B. B. Boonstra, E. M. Dannenberg, and F. A. Heckman, Rubber Chem. Technol. **47**, 1082 (1975).
[35] R. Gehrke, Rev. Sci. Instrum. **63**, 455 (1992).
[36] R. Gehrke, M. Bark, D. Lewin, and S. Cunis, Rev. Sci. Instrum. **66**, 1354 (1995).
[37] S. K. Friedlander, K. Ogawa, and M. Ullmann, J. Polym. Sci., Part B: Polym. Phys. **38**, 2658 (2000).
[38] S. K. Friedlander, K. Ogawa, and M. Ullmann, Powder Technol. **118**, 90 (2001).
[39] Y. J. Suh and S. K. Friedlander, J. Appl. Phys. **93**, 3515 (2003).
[40] W. Rong, A. E. Pelling, A. Ryan, J. K. Gimzewski, and S. K. Friedlander, Nano Lett. **4**, 2287 (2004).
[41] R. Hosemann and S. N. Bagchi, *Direct Analysis of Diffraction by Matter* (North-Holland, Amsterdam, 1962).
[42] B. B. Mandelbrot, *The Fractal Geometry of Nature* (W. H. Freeman, New York, 1977).
[43] M. K. Wu and S. K. Friedlander, J. Colloid Interface Sci. **159**, 246 (1993).
[44] V. I. Roldughin, Russ. Chem. Rev. **72**, 823 (2003).
[45] C. Oh and C. M. Sorensen, J. Coll. Interface Science **193**, 17 (1997).
[46] G. Beaucage, D. W. Schaefer, T. Ulibarri, and E. Black, Polym. Mater. Sci. Eng. **70**, 268 (1993).
[47] A. Hasmy, R. Vacher, and R. Jullien, Phys. Rev. B **50**, 1305 (1994).
[48] R. Jullien, J. Phys. France **2**, 759 (1992).
[49] D. W. Schaefer, C. Suryawanshi, P. Pakdel, J. Ilavsky, and P. R. Jeminan, Physica A **314**, 686 (2002).
[50] G. Beaucage, H. K. Kammler, and S. E. Pratsinis, J. Appl. Crystallogr. **37**, 523 (2004).
[51] H. Peterlik and P. Fratzl, Monatsh. Chem. **137**, 529 (2006).
[52] J. Oberdisse, Y. Rharbi, and F. Boué, Comput. Theor. Polym. Sci. **10**, 207 (2000).